Nanoscale Research Letters
a SpringerOpen Journal

NANO EXPRESS Open Access

Role of vanadium ions, oxygen vacancies, and interstitial zinc in room temperature ferromagnetism on ZnO-V_2O_5 nanoparticles

Sion F Olive-Méndez[1*], Carlos R Santillán-Rodríguez[1], Ricardo A González-Valenzuela[2], Francisco Espinosa-Magaña[1] and José A Matutes-Aquino[1]

Abstract

In this work, we present the role of vanadium ions (V^{+5} and V^{+3}), oxygen vacancies (V_O), and interstitial zinc (Zn_i) to the contribution of specific magnetization for a mixture of ZnO-V_2O_5 nanoparticles (NPs). Samples were obtained by mechanical milling of dry powders and ethanol-assisted milling for 1 h with a fixed atomic ratio V/Zn = 5% at. For comparison, pure ZnO samples were also prepared. All samples exhibit a room temperature magnetization ranging from 1.18×10^{-3} to 3.5×10^{-3} emu/gr. Pure ZnO powders (1.34×10^{-3} emu/gr) milled with ethanol exhibit slight increase in magnetization attributed to formation of Zn_i, while dry milled ZnO powders exhibit a decrease of magnetization due to a reduction of V_O concentration. For the ZnO-V_2O_5 system, dry milled and thermally treated samples under reducing atmosphere exhibit a large paramagnetic component associated to the formation of V_2O_3 and secondary phases containing V^{+3} ions; at the same time, an increase of V_O is observed with an abrupt fall of magnetization to $\sigma \sim 0.7 \times 10^{-3}$ emu/gr due to segregation of V oxides and formation of secondary phases. As mechanical milling is an aggressive synthesis method, high disorder is induced at the surface of the ZnO NPs, including V_O and Zn_i depending on the chemical environment. Thermal treatment restores partially structural order at the surface of the NPs, thus reducing the amount of Zn_i at the same time that V_2O_5 NPs segregate reducing the direct contact with the surface of ZnO NPs. Additional samples were milled for longer time up to 24 h to study the effect of milling on the magnetization; 1-h milled samples have the highest magnetizations. Structural characterization was carried out using X-ray diffraction and transmission electron microscopy. Identification of V_O and Zn_i was carried out with Raman spectra, and energy-dispersive X-ray spectroscopy was used to verify that V did not diffuse into ZnO NPs as well to quantify O/Zn ratios.

Keywords: Vanadium ions; Oxygen vacancies; Interstitial zinc; Room temperature ferromagnetism; V-doped ZnO

Background

The complex mechanisms that allow ferromagnetic order at room temperature in diluted magnetic oxides (DMO) are a controversial subject as magnetic behavior is strongly dependent on the synthesis method and it is very difficult to obtain reproducible homogeneity on samples. It has been widely supported that ferromagnetism is originated by structural defects [1,2], mainly oxygen vacancies [3], but there exist some other structural defects such as interstitial cations [1,4], cation vacancies [5], impurities [6], and if we consider so, the common doping with 3d ions [7]. It has been shown theoretically and experimentally ([8] and references there in, [9]) that almost all of these defects have magnetic moment. On the other hand, some other systems report the absence of room temperature ferromagnetism on the same material combination. Coey et al. reported the construction of a phase diagram [10] for DMO, including percolation thresholds for oxygen vacancies (V_O) and doping cations. Depending on the combination of these important defects, ferromagnetic, paramagnetic, or antiferromagnetic order can be presented on semiconducting or insulating oxides. Structural disorder can also be present

* Correspondence: sion.olive@cimav.edu.mx
[1]Centro de Investigación en Materiales Avanzados, S. C., CIMAV, Av. Miguel de Cervantes 120, Complejo Industrial Chihuahua, Chihuahua, Chihuahua 31109, Mexico
Full list of author information is available at the end of the article

in epitaxial thin films where crystalline order does not mean absence of Schottky and Frenkel defects. Epitaxial films are normally grown under thermodynamic equilibrium, avoiding an excessive formation of punctual defects higher than that intrinsically found: interstitial cations or V_O in ZnO, TiO_2, or SnO_2.

The most popular mechanism for ferromagnetic order in DMO is the bound magnetic polaron (BMP) where a trapped electron at the site of the V_O, with a hydrogenic radius (0.4 to 0.6 nm), intercepts and polarizes the magnetic moment from 3d ions creating ferromagnetic order. Percolation of such BMPs creates a spin-polarized impurity band. The polarization of this band depends on the energetic overlapping with the spin split 3d bands of the cation. This is a reason which holds that no ferromagnetism would be expected for certain systems such as SnO_2: Sc, Ti, and Zn [3] or ZnO: Cr [11]. On the other hand, ferromagnetism evidence on SnO_2:Zn nanorods [12] was recently reported. It was proposed that substitutional Zn induced the formation of Sn_i defects to which is attributed the magnetic moment. This model is reinforced by theoretical calculations carried out by several groups [13,14]. The model used to refer the origin of magnetism based on interstitial cations is named BMP' [15]. Structural defects do not mean partially amorphous material, but a concentration of punctual defects in monocrystalline structures.

In this paper, we report results concerning the structural and magnetic behavior of pure ZnO NPs milled under different conditions, and on the second part, we present a complete analysis of ZnO-V_2O_5 NPs, getting a clear conclusion about the role of each structural defect.

Methods

Samples were obtained by mechanical milling using a high-energy SPEX mill (Spex Industries, Inc., Metuchen, NJ, USA) for 1, 8, and 24 h on a polymer jar with yttrium-stabilized zirconia balls. Powders 99.9% ZnO and 99.6% V_2O_5 (both from Sigma-Aldrich, St. Louis, MO, USA) were used on the stoichiometric proportion to have 5% at. of V atoms against the total amount of metallic atoms. Also, pure ZnO powders were milled for 1 h with and without ethanol to evaluate the contribution from interstitial zinc (Zn_i) to the magnetic moment of the samples. Thermal treatment under reducing atmosphere (TT), a mixture of Ar:H_2 [10:1], at 680°C for 1 h was applied to some of the obtained samples, a temperature barely higher than 672°C, which is the V_2O_5 melting point. This temperature was selected to ensure reaction between H_2 and O from ZnO to produce V_O. Magnetic σ(H) measurements were performed for all samples with a physical properties measuring system (PPMS) from Quantum Design (San Diego, CA, USA) at room temperature and an applied field of 2 T. Structural characterization was obtained from X-ray diffraction patterns (XRD). Chemical composition was identified by energy-dispersive X-ray spectroscopy (EDS) from EDAX in a transmission electron microscope (TEM) and in form of green compressed pellets in a scanning electron microscope (SEM). Micro-Raman spectroscopy was used to identify the presence of V_O and Zn_i.

To name the samples, we use the following nomenclature: for ZnO-V_2O_5 samples, a number followed by letter *h* will be used to identify milling time. Ethanol-milled samples will have the suffix *.Et*, while dry milled samples do not have any suffix. Thermally treated samples will have. *Cal* suffix. Sample ZnO.Com represents commercial ZnO powder without any treatment. For example, sample 1 h.Et.Cal is a mixture of ZnO and V_2O_5 milled for 1 h with ethanol followed by TT, while ZnO. Et is pure ZnO ethanol-milled for 1 h and ZnO is 1-h dry milled ZnO.

Results and discussion

Pure ZnO nanoparticles

Pure ZnO NPs were mechanically milled for 1 h with and without ethanol, samples ZnO.Et and ZnO, respectively. XRD patterns (not shown) for these samples and also from sample ZnO.Com show the wurtzite crystal structure; the only difference is related to the peak width. Using Scherrer formula, NPs from sample ZnO have an average size of 26 nm, while samples ZnO.Et and ZnO.Et.Cal measure 42 nm. Particles from sample ZnO.Com have an average size of 5 μm. The effect of mechanical milling on the creation of structural defects such as Zn_i and V_O on the NPs was evaluated by micro-Raman spectroscopy, as shown in Figure 1 for all samples. The modes corresponding to bulk ZnO that appear in our NPs are E_2(high), A_1(TO), and E_1(TO), which are

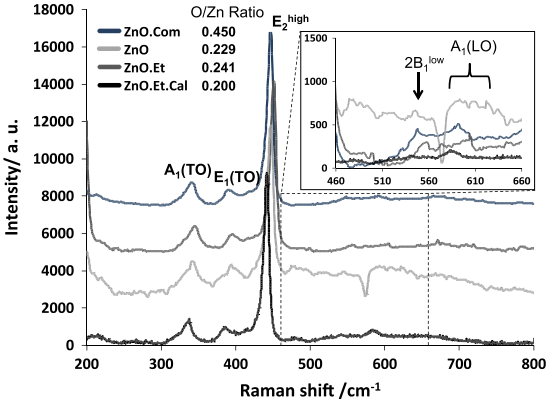

Figure 1 Raman spectra of pure ZnO samples under different synthesis conditions. Samples ZnO.Com, ZnO.Et, ZnO, and ZnO.Et.Cal. Sample ZnO (dry milled) has very different behavior than the rest of the samples; additional peaks are attributed to Zn_i impurity complexes.

representative of a wurtzite structure. Of particular interest are A_1 modes that are related to defects such as V_O and Zn_i. On sample ZnO, A_1(LO) mode at 590 cm^{-1} has the higher intensity that can be attributed to Zn_i and not to V_O as the sample was dry milled, and oxygen atoms at the surface limit formation of these latest defects. Spectra from samples ZnO.Com and ZnO.Et are very similar; only a reduction on the intensity of the peaks and a small shift are observed, assuming that only a change on the surface bonds of the NPs attributed to size change is reflected. Zn_i has a diffusion barrier of 0.57 eV [16] that makes it unstable at room temperature. However, it has been proposed that complexes involving N impurities could be stable at room temperature [17]. Ethanol milling avoided the adhesion of oxygen atoms at the surface of the NPs; thus, V_O concentration may remain stable. The effect of dry milling, ethanol milling, and TT on the stoichiometry of the samples is reflected on the O/Zn ratios obtained from EDS (Figure 1 next to sample labels).

Magnetic σ(H) loops, for all samples except for ZnO. Et.Cal, are shown in Figure 2 after subtraction of all diamagnetic components arising from the container and from nonferromagnetic ZnO. Sample ZnO.Com is expected to be completely diamagnetic; however, it has a magnetization of 1.34×10^{-3} emu/gr, attributed to a small amount of Zn_i and impurities of the material, as it is not a high-purity material. The inset of Figure 2 shows the first and fourth quadrant of the as-measured σ(H) loops; the lower absolute value of the slope of the diamagnetic component for sample ZnO.Com can be interpreted as concentration of randomly distributed impurities and Zn_i leading to a small diamagnetic component of ZnO. The increase of the absolute value of the slope after milling implies atom diffusion that increases the pure diamagnetic ZnO in the core of the NPs and a significant increase of Zn_i defects at the shell that are the sources of magnetic moment. For sample ZnO, oxygen from air during milling is in direct contact with NP surface; this implies a chemical potential of O_2 that reduces the concentration of V_O. Even if milling induces structural disorder and thus increase of Zn_i, the total amount of V_O, which mediates ferromagnetic order, decreases and then magnetization falls to 1.18×10^{-3} emu/gr.

For sample ZnO.Et, the O_2 chemical potential is eliminated as the NPs are surrounded by ethanol molecules. Then, the amount of V_O is kept constant while milling increases the concentration of Zn_i (source of magnetic moment); as a consequence, magnetization increases from 1.34×10^{-3} (ZnO.Com) to 1.42×10^{-3} emu/gr. There exist some reports that attribute ferromagnetic signal in DMO only to V_O, but with these defects even if they have magnetic moment (as a consequence of antiferromagnetic coupling with the sources of magnetism: interstitial cations of 3d dopants [18,19]), the role of V_O is only to mediate ferromagnetic order between magnetic moment sources and not to produce magnetic signal. For pure oxide systems, the used model is the BMP'. Our samples were used to confirm the existence of Zn_i defects at which we attribute the ferromagnetic enhancement magnetization by ethanol-assisted mechanical milling.

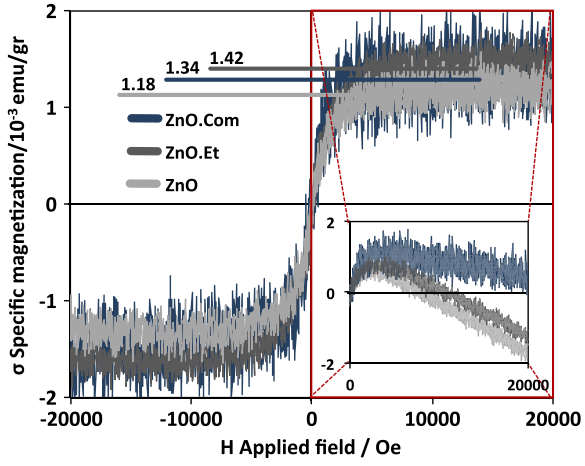

Figure 2 Magnetic σ(H) loops performed at room temperature compared with commercial powders. The increase of magnetization on sample ZnO.Et is attributed to formation of Zn_i, while its reduction on sample ZnO is attributed to a reduction of V_O. The inset represents the first and fourth quadrants including the diamagnetic component of M(H) loops as obtained from the PPMS. The lower value of the diamagnetic component on sample ZnO.Com suggests that Zn_i is randomly distributed in the whole particle.

ZnO-V_2O_5 nanoparticles

Identification of ZnO, V_2O_5, and secondary phases of all ZnO-V_2O_5 samples was carried out by XRD patterns shown in Figure 3. One of the most stable V oxides besides V_2O_3 is V_2O_5; both of them have affinity to form secondary phases with ZnO [20]. On sample 1 h, only the wurtzite structure of ZnO is observed, suggesting that dry milling reduces the size of V_2O_5 powders in order to make them undetectable for XRD. Using Scherer formula, ZnO NPs on this sample have an average size of 24 nm, while NPs from sample 1 h.Et (and samples after TT) have an average size of 45 nm, demonstrating that ethanol-assisted milling is more gentle with powders; also, small peaks corresponding to V_2O_5 are found on XRD pattern of sample 1 h.Et. Diffraction patterns of samples after TT (1 h.Cal and 1 h.Et.Cal) reveal the existence of V_2O_5 and the formation of γ-$Zn_3(VO_4)_2$ and ZnV_2O_4 secondary phases which are the products of the reaction of ZnO with V_2O_5 and V_2O_3 after TT [20]. On the same figure, next to each sample label, the chemical composition features obtained by EDS - the V at. % and the O/Zn ratio - are shown; the

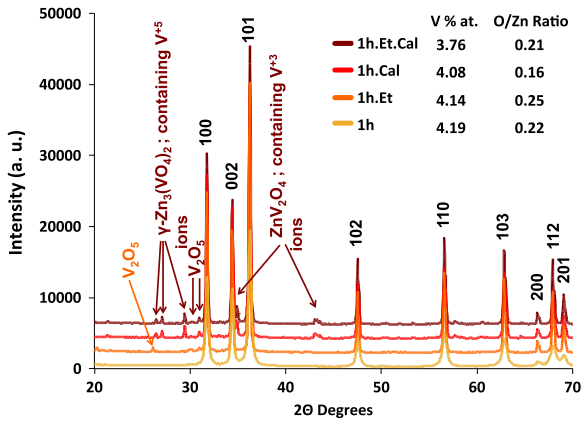

Figure 3 XRD patterns for all ZnO-V_2O_5 samples showing the wurtzite structure of ZnO. Additional peaks corresponding to V_2O_5, and secondary phases for some milling and TT processes. Near the sample labels, qualitative stoichiometric features of the samples are presented.

last one reduces after each TT, demonstrating an increase of V_O concentration.

Figure 4 is a TEM micrograph of a NP from sample 1 h where the nominal V composition is 5% at. EDS line profiles of Zn, O, and V were obtained along the NP where the V profile is a constant line without any intensity change even in the thicker zones of the NP; we suggest that V oxide NPs are surrounding the ZnO NP. Milling process only reduces the particle size and favors the contact between both oxides at the surface of ZnO NPs, but no V diffusion is observed into the ZnO.

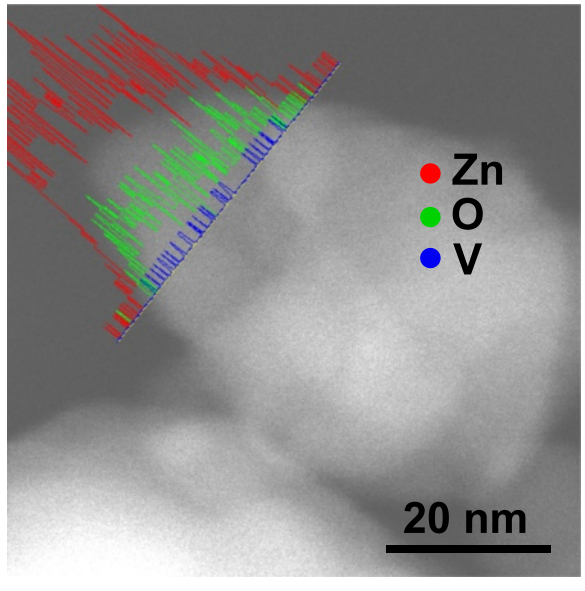

Figure 4 TEM micrograph of a NP from sample 1 h. The continuous V profile demonstrates that V atoms are surrounding the ZnO NP and no V diffusion into the NP is observed.

Magnetic σ(H) loops for all 1-h milled samples are shown in Figure 5a. Sample 1 h has a very strong paramagnetic component that only can be attributed to V_2O_3 formation, which has a paramagnetic susceptibility equal to 13.184×10^{-6} cm^3/gr which is larger than that of V_2O_5, $X_{V2O5} = 0.703 \times 10^{-6}$ cm^3/gr. It is possible that V ions were reduced through the reaction $V^{+5} + 2e^- \rightarrow V^{+3}$ where the electrons can be taken from the free electron pairs of oxygen from air, representing a chemical potential for this reaction. The spin-only magnetic moment of V^{+3} is 2.83 μ_B/ion, while V^{+5} should be completely diamagnetic. Sample 1 h.Et has a weak paramagnetic component attributed to the lack of reduction of V^{+5} ions (absence of oxygen surrounding V_2O_5 NPs); by XRD, we only detect

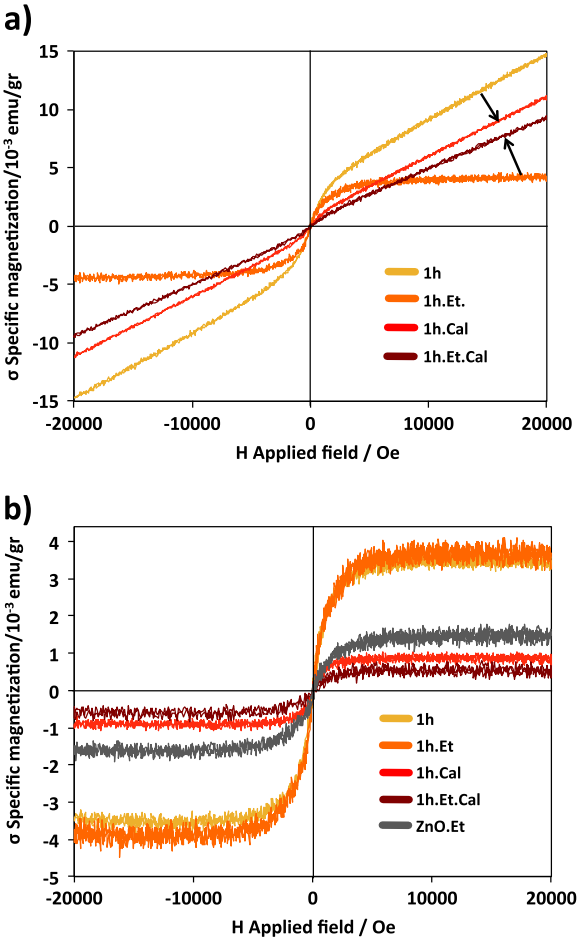

Figure 5 Magnetization loops performed at room temperature showing paramagnetic and ferromagnetic components. (a) Specific magnetization loops σ(H) for all ZnO-V_2O_5 samples after subtracting the diamagnetic component from the container. A strong paramagnetic component appears on samples 1 h, 1 h.Cal, and 1 h.Et.Cal which is attributed to the formation of V_2O_3 on sample 1 h, and secondary phases containing V^{+3} ions on samples 1 h.Cal and 1 h.Et.Cal. The arrows show how the paramagnetic component changes after TT. **(b)** Ferromagnetic components produced by $V^{+5,\ +3}$ ions and V_O near the surface of the ZnO NPs to form BMPs.

V_2O_5. These paramagnetic-diamagnetic components for samples 1 h and 1 h.Et are consistent with the previous explanation from XRD patterns, where almost all V_2O_5 is transformed in very small V_2O_3 NPs for sample 1 h with high paramagnetic susceptibility, while sample 1 h.Et (less aggressive milling) has a significant amount of V_2O_5, reducing the value of the paramagnetic slope in Figure 5b.

Samples with TT have a reduction of the O/Zn ratio as a consequence of the creation of V_O; these ratios are semiqualitative as EDS is not a completely quantitative technique. There is also a reduction of the V concentration as a consequence of V_2O_5 evaporation.

Secondary phase formation containing V^{+3} ions for samples with TT is also supported by the high positive susceptibility measured on samples; the arrows in Figure 5a indicate the direction in which the susceptibility from samples 1 h and 1 h.Et has changed after TT, supporting the idea that γ-$Zn_3(VO_4)_2$ and ZnV_2O_4 are formed during TT and/or cooling and not during milling. A combination of diamagnetic susceptibility from ZnO and paramagnetic susceptibility from γ-$Zn_3(VO_4)_2$ and ZnV_2O_4 contributes to the approached value (arrows in Figure 5a). The paramagnetic change is stronger on sample 1 h.Et.Cal, which has lower V_2O_3 content after milling; then, the TT reduced some of the V^{+5} to V^{+3} ions and both of the secondary phases are formed. For sample 1 h, the behavior turns on the opposite way; susceptibility has a slight decrement suggesting separation of V_2O_3 NPs from ZnO surface to form secondary phases and V_2O_5.

Ferromagnetic components from typical DMO mechanisms for all samples are shown in Figure 5b. Samples 1 h and 1 h.Et have the highest specific magnetizations $\sigma \sim 3.5 \times 10^{-3}$ emu/gr, but as sample 1 h has the largest paramagnetic component, attributed to V_2O_3, we can assume that not all V^{+5} or V^{+3} contribute to the ferromagnetic moment on the samples. Usually high doping concentration of magnetic ions forms antiferromagnetic complexes [21]; this is the reason that lower ion concentration produces the highest magnetic moment per doping ion. As V has a very low solubility limit on ZnO ~ 0.2% [22], secondary phases are more easily formed instead of promotion of V diffusion into the ZnO matrix. After TT magnetization decays to $\sigma \sim 0.7 \times 10^{-3}$ emu/gr, which has been already explained with the formation of secondary phases and is also due to a reduction of structural defects on ZnO, NPs from sample 1 h increase their average size by coalescence to reduce their surface free energy and a reorganization of the surface is promoted by atom diffusion, reducing the sources of magnetism; at the same time, reaction between ZnO and V oxides produces secondary phases, reducing the number of ZnO/V interfaces.

Raman spectra of ZnO-V_2O_5 NPs are shown in Figure 6; for samples 1 h.Et and 1 h.Et.Cal, it is very clear that the set of peaks at 200 to 380 and 780 to 1,000 cm^{-1} belong to ZnV_2O_4 phase, and this result is consistent with previous XRD patterns of the same samples. Sample 1 h has two peaks (weak and broad) located near the regions were the ZnV_2O_4 phase was identified. Peaks from sample 1 h.Et does not match with any of the previous cases, as this sample is the only one that does not exhibit paramagnetic component; peaks must correspond to V_2O_5 NPs. All spectra are compared with a pure ZnO sample milled with ethanol and thermally treated.

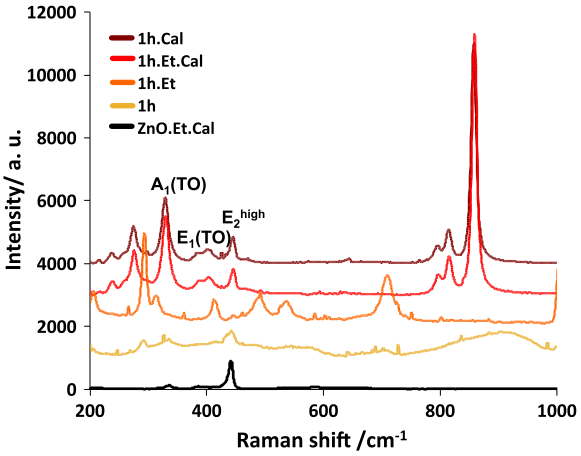

Figure 6 Raman spectra of ZnO-V_2O_5 nanoparticles with and without thermal treatment. Samples 1 h.Cal and 1 h.Et.Cal exhibit a strong paramagnetic component attributed to the formation of secondary phases containing V^{+3} ions. The peaks in the intervals 200 to 360 and 780 to 1,000 cm^{-1} are attributed to ZnV_2O_4 phase. The weak and broad peaks for sample 1 h centered at 420 and 900 cm^{-1} are attributed to amorphous material linked to V^{+3} ions.

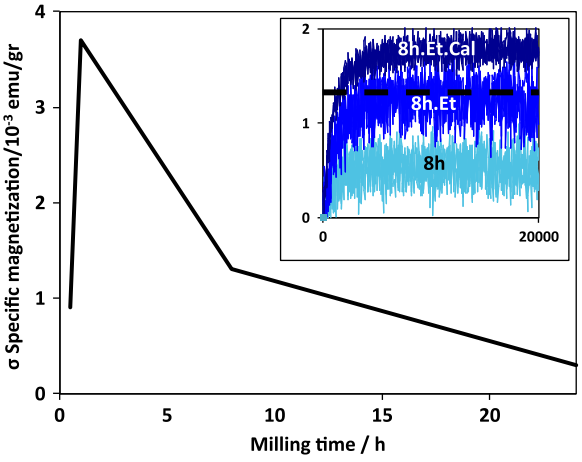

Figure 7 Variation of saturation magnetization depending on milling time. The maximum for our synthesis parameters was found around 1 h. The inset shows how the TT increased the magnetic moment for samples milled for 8 h. Probably, long-time milling contributes to reduce intrinsic V_O on ZnO, thus reducing the defects that mediate ferromagnetic order.

Dry milling produces a size reduction of V_2O_5 powders, but no phase change is involved. On sample 1 h, a small amount of V_2O_5 is used to produce magnetic moment; the rest is transformed to V_2O_3. We conclude that there exists a threshold concentration for which larger concentrations of magnetic ions do not help to increase the magnetic signal. No antiferromagnetic coupling is observed. To verify this fact, powders where milled with and without ethanol for 8 h to reduce particle size and increase the ZnO/V interface area; then, TT was applied for the 8 h.Et sample. Average particle sizes determined by Scherer formula are 19 and 45 nm for samples 8 h and 8 h.Et, respectively, reducing the particle size only for dry milled sample. Magnetization σ(H) loops (first quadrant) are shown in the inset of Figure 7. Here the TT enhances the saturation magnetization, but all magnetizations are smaller than that of sample 1 h.Et. Probably, long-time milling contributes to reduce intrinsic V_O on ZnO by reduction of V^{+5} ions. In Figure 7, a variation of saturation magnetization depending on milling time is shown. The maximum depends on the mass of the milled powders, the amount of ethanol, the size of the jar, and the number and size of the milling media, reinforcing the idea that ferromagnetism in DMO is not trivial and synthesis conditions are critical in order to maximize magnetic moment of the samples.

Conclusions

We prepared pure ZnO and a mixture of ZnO and V_2O_5 NPs by mechanical milling in different conditions: dry and ethanol-assisted milling. From Raman spectra of the pure ZnO dry milled sample, the increase of the signal of the A_1(LO) mode, related to structural defects such as Zn_i, supports the fact that this defect is the source of magnetic moment as the sample has higher magnetization than that of commercial ZnO. On the other hand, dry milled samples exhibit a reduction of magnetization; even if milling increases the concentration of Zn_i, the exposure of the powders to oxygen from air during milling reduces the amount of V_O, which mediates ferromagnetic order between Zn_i. The coupling between Zn_i through V_O corresponds to the BMP' model.

For the ZnO-V_2O_5 system, it was proven that V^{+5} ions added at the surface of the ZnO NPs form BMPs, increasing the magnetization from 1.42×10^{-3} to 3.5×10^{-3} emu/gr, demonstrating that V ions produces magnetic order in the system ZnO:V. TT induced the formation of ZnV_2O_4 secondary phase, containing V^{+3} ions, which is paramagnetic. V^{+3} ions are also present on ZnO-V_2O_5 dry milled sample as shown by a weak and broad peak on Raman spectra on the interval 750 to 1,000 cm^{-1}, supporting the idea that dry milling, in some form, reduces the charge of some ions from V^{+5} to V^{+3}. After TT, the amount of V_O was increased but magnetization falls to 0.7×10^{-3}, demonstrating that the intrinsic amount of V_O on ZnO is enough to mediate ferromagnetic order.

Competing interests

The authors declare that they have no competing interests.

Authors' contributions

SFOM made all the NP samples, performed data interpretation, and worked on the manuscript. CRSR performed magnetic measurements. RAGV participated in Raman interpretation and financial facilities. FEM worked on the manuscript, and JAMA participated in acquiring the magnetic loops facilities. All authors read and approved the final manuscript.

Authors' information

All authors work at CIMAV Chihuahua, with the exception of RAGV who works at Honeywell Chihuahua as a design engineer. SFOM is working as a researcher in the field of nanostructured and magnetic materials. CRSR is working as a technician in charge of several magnetic measuring techniques. FEM is a professor working with theoretical simulation, and JAMA is a professor working with a wide variety of magnetic materials.

Acknowledgements

The authors thank the financial support received from PROIN-CONACYT grant no. 197000. Also want to thank Karla Campos Venegas for EDS acquisition, Enrique Torres Moye for XRD patterns, and Pedro Pizá Ruiz for Raman acquisition.

Author details

[1]Centro de Investigación en Materiales Avanzados, S. C., CIMAV, Av. Miguel de Cervantes 120, Complejo Industrial Chihuahua, Chihuahua, Chihuahua 31109, Mexico. [2]Honeywell Manufacturas de Chihuahua, S de RL de CV, Chihuahua, Chihuahua 31136, Mexico.

Received: 17 January 2014 Accepted: 29 March 2014
Published: 7 April 2014

References

1. Das Pemmaraju C, Sanvito S: **HfO_2: a new direction for intrinsic defect driven ferromagnetism.** *Phys Rev Lett* 2005, **94:**217205–217208.
2. Xu Q, Zhou S, Schmidt H: **Magnetic properties of ZnO nanopowders.** *J Alloys Compd* 2009, **487:**665–667.
3. Fitzgerald CB, Venkatesan M, Dorneles LS, Gunning R, Stamenov P, Coey JMD, Stampe PA, Kennedy RJ, Moreira EC, Sias US: **Magnetism in dilute magnetic oxide thin films based on SnO_2.** *Phys Rev B* 2006, **74:**115307.
4. Xu Z, Soack-Dae Y, Aria Y, Wen-Hui D, Carmine V, Vincent GH: **Ferromagnetism in pure wurtzite zinc oxide.** *J Appl Phys* 2009, **105:**07C508-1-3.
5. Khalid M, Ziese M, Setzer A, Esquinazi P, Lorenz M, Hochmuth H, Grundmann M, Spemann D, Butz T, Brauer G, Anwand W, Fischer G, Adeagbo WA, Hergert W, Ernst A: **Defect-induced magnetic order in pure ZnO films.** *Phys Rev B* 2009, **80:**035331-1-5.
6. Ackland K, Monzon LM, Venkatesan M, Coey J: **Magnetism of nanostructured CeO_2.** *IEEE Trans on Mag* 2011, **47:**3509–3512.
7. Pan F, Song C, Liu XJ, Yang YC, Zeng F: **Ferromagnetism and possible application in spintronics of transition-metal-doped ZnO films.** *Mat Sci and Eng R* 2008, **62:**1–35.
8. Coey JMD, Stamenov P, Gunning RD, Venkatesan M, Paul K: **Ferromagnetism in defect-ridden oxides and related materials.** *New J Phys* 2010, **12:**053025.
9. Fan L, Dongmei J, Xueming M: **The influence of annealing on the magnetism of Fe-doped ZnO prepared by mechanical alloying.** *Physica B* 2010, **405:**1466–1469.
10. Coey JMD, Venkatesan M, Fitzgerald CB: **Donor impurity band exchange in dilute ferromagnetic oxides.** *Nature Mat* 2005, **4:**173–179.
11. Coey JMD, Wongsaprom K, Alaria J, Venkatesan M: **Charge-transfer ferromagnetism in oxide nanoparticles.** *J Phys D Appl Phys* 2008, **41:**134012-1-6.
12. Liu X, Iqbal J, Wu Z, He B, Yu R: **Structure and room-temperature ferromagnetism of Zn-doped SnO_2 nanorods prepared by solvothermal method.** *J Phys Chem C* 2010, **114:**4790–4796.
13. Schlenkera E, Bakina A, Postelsa B, Mofora AC, Kreyea M, Ronningb C, Sieversc S, Albrechtc M, Siegnerc U, Klingd R, Waaga A: **Magnetic**

characterization of ZnO doped with vanadium. *Superlattices Microstruct* 2007, **42:**236–241.
14. Das J, Pradhan SK, Mishra DK, Sahu DR, Sarangi S, Varma S, Nayak BB, Jow-Lay H, Roul BK: **Unusual ferromagnetism in high pure ZnO sintered ceramics.** *Mater Res Bull* 2011, **46:**42–47.
15. Panguluri RP, Kharel P, Sudakar C, Naik R, Suryanarayanan R, Naik VM, Petukhov AG, Nadgorny B, Lawes G: **Ferromagnetism and spin polarized charge carriers in In_2O_3 thin films.** *Phys Rev B* 2009, **79:**165208–165213.
16. Janotti A, Van de Walle CG: **Native point defects in ZnO.** *Phys Rev B* 2007, **76:**165202–165223.
17. Look DC, Farlow GC, Reunchan P, Limpijumnong S, Zhang SB, Nordlund K: **Evidence for native-defect donors in n-type ZnO.** *Phys Rev Lett* 2005, **95:**225502.
18. Durst AC, Bhatt RN, Wolff PA: **Bound magnetic polaron interactions in insulating doped diluted magnetic semiconductors.** *Phys Rev B* 2002, **65:**235205-1-11.
19. Coey JMD, Douvalis AP, Fitzgerald CB, Venkatesan M: **Ferromagnetism in Fe-doped SnO_2 thin films.** *Appl Phys Lett* 2004, **84:**1332–1334.
20. Kurzawa M, Rychlowska-Himmel I, Bosacka M, Blonska-Tabero A: **Reinvestigation of phase equilibria in the V_2O_5-ZnO system.** *J Therm Anal Calorim* 2001, **64:**1113–1119.
21. Jedrecy N, Von Bardeleben HJ, Zheng Y, Cantin JL: **Electron paramagnetic resonance study of $Zn_{1-x}Co_xO$: a predicted high-temperature ferromagnetic semiconductor.** *Phys Rev B* 2004, **69:**041308.
22. Jung-Joo K, Tae-Bong H, Jin Sung K, Dae Young K, Yoon-Hwae H, Hyung-Kook K: **Solubility of V_2O_5 in polycrystalline ZnO with different sintering conditions.** *J Korean Phys Soc* 2005, **47:**S333–S335.

doi:10.1186/1556-276X-9-169
Cite this article as: Olive-Méndez *et al.*: Role of vanadium ions, oxygen vacancies, and interstitial zinc in room temperature ferromagnetism on ZnO-V_2O_5 nanoparticles. *Nanoscale Research Letters* 2014 **9**:169.